First principle studies of oxygen reduction reaction on N doped graphene: Impact of N concentration, position and co-adsorbate effect

Applied Surface Science 510 (2020) 145470

Contents lists available at ScienceDirect

Applied Surface Science

journal homepage: www.elsevier.com/locate/apsusc

Full Length Article

First principle studies of oxygen reduction reaction on N doped graphene: Impact of N concentration, position and co-adsorbate effect

Isabela-Costinela Man[a,*], Ionut Trancă[b,*], Stefan-Gabriel Soriga[a]

[a] Romanian Academy, "C.D. Nenitzescu" Center of Organic Chemistry, 202B Spl. Independentei, RO-060023 Bucharest, Romania
[b] Energy Technology, Department of Mechanical Engineering, Eindhoven University of Technology, 5600 MB Eindhoven, The Netherlands

ARTICLE INFO

Keywords:
DFT
Graphene
Nitrogen
ORR

ABSTRACT

Density Functional Theory calculations were performed on N doped graphene sheet to investigate the trends for adsorption energy variation of oxygen reduction reaction intermediates (HOO*, O*, HO*) when the N concentration increases from 0N (0%) to 1N (33%), to 2N (67%) and to 3N (100%) around the C active site. The impact of the distance between the doping N atoms and the C active site is also studied. Last, the impact of additionally co-adsorbed HO*/O* intermediates was probed. For all the studied systems the magnitudes with which varies the adsorption energies are shaped by the HO*/HOO* capability of accommodating less charge than O* (i.e according to octet rule $1e^-$ vs. $2e^-$). When N concentration increases, adsorption energy of O* increases with a much higher magnitude than that of HO*/HOO* (i.e with 5 eV vs. 2.7 eV, when going from 0N to 3N). In the presence of the O* co-adsorbate, adsorption energy of intermediates on the investigated active site decrease with a much higher magnitude than when 1HO* is present as co-adsorbate (≈2 eV vs. 1 eV). The theoretical overpotential trends are evaluated using ΔG_{HO*}-ΔG_{O*} descriptor and are found to be significantly influenced by all these environmental changes around the active site. By applying the water stabilization effects, the activity trends remain the same as when it is not taken into account. These results reveal aspects of ORR activity variations that take place when N is clustering on graphene sheets, structures that can be possible as a function of synthesis procedures that could lead to unevenly distribution of dopants in the matrix.

1. Introduction

Nitrogen is an ideal candidate for doping graphene and other graphitic materials (eg. nanotubes) because the C—N bond length is comparable with the C—C bond and the distortion of graphene lattice upon doping is relatively small, which makes it the most well studied dopant in graphene. The bonding configuration around N (graphitic-N, pyridinic-N, pyrrolic-N) changes sensitively with the synthesis conditions (ex. used methods, temperatures, source molecules, etc.), therefore an inhomogeneous distribution of incorporated N in the N-doped materials is expected and can be shaped experimentally [1,2]. The experimental studies and their techniques can be directed to manipulate the exact positioning of doping elements in the graphene matrix to achieve the desired activity as a function of the bonding configuration around the N dopant.

Cathodic electrochemical oxygen reduction reaction (ORR) is the application for which the nitrogen doped graphitic materials were shown to exhibit activities [3–6] and are one of the materials that are considered to be replacement for the expensive/scarce Pt based materials. ORR represents the bottleneck in the low temperature fuel cells to realize their large scale commercialization, due to sluggish kinetics and high overpotentials [7]. These devices are recognized as one of the most attractive alternatives to combustion engines for automotive applications [8]. Therefore designing proper catalysts from all points of view (activity, selectivity, price, resistance in time, etc.) is of tremendous importance.

With the aid of theoretical approaches, it was shown that the active site for ORR, is the C atom adjoining a N atom [9]. This is explained by the fact that the electronegative N atom reduces the electron density of the C atoms that bond with the N atom and polarizes the C atoms into C (δ+), making easier the adsorption of O_2 molecule which is the first step in the ORR process. Moreover, it was shown that O_2 is stabilized significantly when water effects are modeled [10]. Different other aspects such as: the type of doping nitrogen (graphitic, pyridinic, pyrrolic) [7,11,12], concentration of N dopants [9,13,14], solvation effects of reaction intermediates [10,13,15], the size and shape of graphene

* Corresponding authors at: Romanian Academy, "C.D. Nenitzescu" Center of Organic Chemistry, 202B Spl. Independentei, RO-060023 Bucharest, Romania (I. Man). Energy Technology, Department of Mechanical Engineering, Eindhoven University of Technology, 5600 MB Eindhoven, The Netherlands (I. Trancă).
E-mail addresses: isabela.traistaru@ccocdn.ro (I.-C. Man), i.tranca@tue.nl (I. Trancă).

https://doi.org/10.1016/j.apsusc.2020.145470
Received 23 September 2019; Received in revised form 22 December 2019; Accepted 19 January 2020
Available online 22 January 2020
0169-4332/

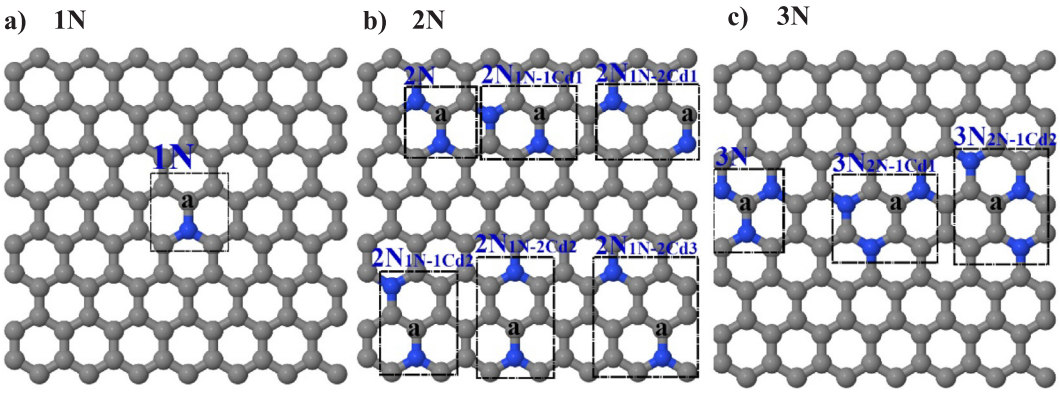

Fig. 1. Illustration of nitrogen distribution around active center in the 8 × 7 zigzag graphene unit cell for (a) 1N (0.89% N concentration), (b) 2N (1.78% N concentration), for which three possible clustering models are explored − 2N type structure (where 2N atoms are adjoining the active site) and $-2N_{1N-1Cd1}$, $2N_{1N-1Cd2}$ type structures – for which N is at 1C site apart from the active site on two directions and − $2N_{1N-2Cd1}$, $2N_{1N-2Cd2}$, $2N_{1N-2Cd3}$ configurations -for which N is at 2C site apart from the active site on three directions) and (c) 3N (2.67% N concentration) with N atoms positioned at several distances from the active site: 3N type structure (all 3N atoms adjoining the active site) and − $3N_{2N-2Cd1}$, $3N_{2N-2Cd2}$ configurations- (where 2N out of 3N atoms are each at 1C site apart from the active site in two distinct directions). The bold letter "**a**" from the figure indicates the position of the active site where the HOO*/O*/HO* intermediates adsorb. Color code – C-gray, N-blue. (For interpretation of the references to color in this figure legend, the reader is referred to the web version of this article.)

sheets were investigated to get insights into activities of these materials [16,17]. Even though in recent years N doped graphitic materials (nanotubes, grapheme, etc.) have been extensively studied for ORR both experimentally and computationally, the active sites and mechanisms are still not completely understood and many aspects needs a deeper understanding, especially when depending on the synthesis procedures the N clustering could take place.

In most DFT studies that imply N concentrations, N is dispersed uniformly in the graphene sheet [13]. On the other hand, Okamoto argued that the concentration of dopant N atoms neighboring the C atom is the key to understanding ORR [9]. On graphene sheets having one to four N impurities in the substitutional site of C, around a C═C bond, he investigated the interaction of O_2 with these sites and showed that the binding interaction between graphene and O_2 becomes stronger as the number of N atoms bonding with the C═C increases. The idea behind the present paper is similar with that of Okamoto's, but there are however main differences between Okamoto's model and the present one. We consider increasing the N concentration inside the basal plane of a very large graphene sheet, right beside the C active site with three possible cases − 1N (33% concentration around the active site), 2N (67%), 3N (100%) with 2N and 3N structures that weren't studied so far in this configuration.

We study the variation of adsorption energy of HOO*/O*/HO* ORR intermediates, while in Okamoto's study the focus was on the first step of O_2 adsorption energy trends. Another major difference is the fact that our N configurations are placed in a very large unit cell compared to Okamoto's– (112 C unit cell vs. 32) such as to act as an island, and be sure that there are no effects related to interactions between periodic images. This is especially important for the surface models when one or two N atoms in 2N and 3N systems are displaced in different directions at 1C/2C/3C atoms distance from the active site. This was performed to determine the distance at which the second N starts to have a significantly diminished effect on the adsorption of reaction intermediates, and consequently the system becomes similar with the case of 1N. If locally the concentration is high, when related to the entire graphene sheet the N concentration is low − 0.89% for 1N, 1.78% for 2N and 2.67% for 3N. Despite the fact that are studies that show that the doped edges are active as well [14], in this study we focus only on the nitrogen doping in a basal plane of graphene sheet. This is because depending on the preparation conditions, the number of available doping sites inside the graphene sheets can be larger than in the edge and is expected not to be uniformly distributed on the surface after synthesis. In this respect we consider that there are still features to be understood concerning the activity of N doped basal plane sites, especially if the clustering phenomenon could happen locally during synthesis procedures.

Because the adsorption of ORR reaction intermediates (HOO*/O*/HO*) has large contribution in the overpotential value, the main focus of the study is to investigate the trends in variation of adsorption energies when passing from one surface to the other, another point that makes difference from other studies. A supplementary aspect to which we pay special attention in this study is the presence of co-adsorbates, aspect not investigated in Okamoto's paper and not too much in the literature. For example, to the best of our knowledge the adsorption of co-adsorbate on 1N type structure wasn't investigated so far. This is crucial to be explored since at higher N concentrations there are more and different types of active sites, and under steady state conditions they will be covered with a certain number of reaction intermediates which can affect the adsorption on the neighboring sites and at their turn the overpotential that can decrease or increase the overpotential. Depending on various factors (pH, voltage, etc.) HO* and O* are likely to be co-adsorbed. More co-adsorbates could adjoin the C sites next to N. In this respect 1N structure and part of the 2N type structures are investigated, and trends are established. The co-adsorbate presence is found to influence quite significantly the adsorption of reaction intermediates. Projected density of states (PDOS) and bond order (BO) calculations are used to gain insights into the underlying phenomena of adsorption. A discussion concerning the effect of water layer on the theoretical overpotential is considered, by using values from two literature references. We do not use continuum solvation models for our systems because it was shown that is unable to describe the solvation of O* with sufficient accuracy [13] and the use of explicit H_2O molecules is cost expensive. The last approach is expected to give relatively similar stabilizations with the one that are taken from the literature.

2. Computational methods

All the density functional theory (DFT) computations were done using the Atomic Simulation Environment [18], coupled with the GPAW ab initio simulation package [19].

We used a 8 × 7 (17.04 Å x17.217 Å) supercell of pristine graphene sheet of configuration (G) doped progressively around the active site with 1N, 2N and 3N dopants (see Fig. 1). This is a large unit cell that gives low N concentration relative to the entire unit cell 0.89% for 1N, 1.78% for 2N, 2.67% for 3N (see Fig. 1) –and a large N concentration relative to the active site (the reaction site) − 33% for 1N, 67% for 2N and 100% for 3N. As a consequence, the N clustering behaves like an island relative to the entire unit cell. In 2N and 3N systems, we explored

also the cases when one or two N atoms were positioned further away from the active site. Thus, for the 2N model one of the two N atoms was positioned at 1C atom site from the active center in two directions (see in Fig. 1b – $2N_{1N-1Cd1}$ and $2N_{1N-1Cd2}$, where $1N-1Cd_{1/2}$ subscript means that 1N is at 1C distance from the active site on one of the two directions d_1 or d_2), than at 2C atoms from the active site in three directions ($2N_{1N-2Cd1}$, $2N_{1N-2Cd2}$, $2N_{1N-2Cd3}$ where $1N-2Cd_{1/2/3}$ subscript means that 1N is found at 2C atoms distance from the active site on one of the three considered directions d_1, d_2 d_3 see Fig. 1b) and then at 3C atoms from the active site (for which we considered enough only one direction to be studied $2N_{1N-3Cd1}$ – not shown in Fig. 1b but similar with $2N_{1N-1Cd1}$ and $2N_{1N-2Cd1}$). For the 3N model two of the three N atoms were separated each by 1C atom from the active site along two set of directions ($3N_{2N-1Cd1}$, $3N_{2N-1Cd2}$).

For all the computations a Fermi smearing of electronic occupations with a width of 0.1 eV was used and the k-point sampling of the Brillouin zone was obtained by using a 2x2x1 Monkhorst-Pack grid centered on the gamma (Γ) point [20].

The vacuum layer region, in-between the periodic images of the system on Z direction, was set to 15 Å. The dipole correction was used to decouple the electrostatic potentials on the two sides of the two dimensional structure. The structure relaxation was performed until the maximum force on each atom drops below 0.05 eV/Å. The exchange-correlation functional used was BEEF-vdW, which was proven to be successful in predicting adsorption bond energies on carbon based materials [21].

The free energy corrections for the adsorbed species are based on the quantum mechanical harmonic approximation and calculated vibrational frequencies.

The data for the bond orders (BO) analysis were obtained in combinations with charge files generated by the Vienna ab initio simulations package [22–25]. For all these calculations the PBE exchange and correlation functional and a cutoff energy of 450 eV were employed. No structural or energy trend modifications were obtained when compared with GPAW calculations. The bond orders analysis was obtained by using the Chargemole code [26–28]. Previous studies showed that the DDEC6 based bond order exhibit good reliability and correlation with the adsorption energies on various systems [29,30].

3. Results

3.1. Formation energy of N-doped graphene

Formation energy (E_F) of the eleven N-doped graphene sheets (Fig. 1) relative to nitrogen molecules and graphene was examined according to the equation:

$$E_F = E(G_{C(112-x)Nx}) - - (112-x)\mu_C - 1/2x\mu_{N2} \quad (1)$$

where $E(G_{C(112-x)Nx})$ is the ground state energy of the graphene sheet doped with 1 to 3N atoms in different configurations. We used the total energy of undoped graphene sheet per atom as μ_C and μ_{N2} of nitrogen in gas phase. The formation energies are listed in Table 1 and indicate an endothermic process. The smallest formation energy is that for the 1N doped graphene. When the concentration increase, the formation energy increase with 1.57 eV for 2N configuration and 1.2–1.27 eV for the other 2N structures, with 1.2 when one of the 2N atoms is at approx. 5 Å from the active site (see in Table 1, $\Delta E_{rel,2Nto1N}$). Indeed the structures with the N placed farthest one by each other are the most stable. Even though for our systems the differences between them are not significant.

It is should be noted that the endothermic formation energy is not unusual. These values are predicted as well for similar systems [9]. Using the same formula they obtained for 1N system the formation energy of 1.11 eV. In the same article they indicate that the standard formation energy of pyrazine molecule ($C_4N_2H_4$) is also endothermic (1.44 and 2.03 eV in crystal and in gas phase, respectively [24]).

Table 1
Formation energy of nitrogen doping E_F.

Structures	E_F/eV	$\Delta E_{rel,2N-1N}$ $E_{f(2N)} - E_{f(1N)}$
1N	1.29	–
2N	2.86	1.57
$2N_{1N-1Cd1}$	2.56	1.27
$2N_{1N-2Cd1}$	2.59	1.32
$2N_{1N-1Cd2}$	2.63	1.34
$2N_{1N-2Cd2}$	2.67	1.38
$2N_{1N-2Cd3}$	2.66	1.37
$2N_{1N-3Cd1}$	2.49	1.20
3N	4.68	1.82
$3N_{1N-1Cd1}$	4.38	–
$3N_{1N-1Cd2}$	3.77	–

Definitely is possible to fabricate the less stable models since N_2 gas is not the only way to dope graphene with N. Various aromatic compounds are used to synthesize N doped graphene (i.e. ionic liquids [31]) and once obtained these structures are predicted to be stable as the desorption of N_2 molecule from models is calculated to be highly exothermic (i.e. 11.95 eV [9]). The possibility of synthesizing unevenly distributed N in the graphene matrix is one of the main reason we focused on the system that comprise an island like configuration of N in the graphene sheet.

3.2. Variation of adsorption energies on the surface models

Adsorption energies of the ORR intermediates are the ones that contribute the most to the overpotential value and are defined as the DFT energies of the following reactions:

$$H_2O + * \rightarrow O^* + H_2, \quad \Delta E_{ads,O^*} = E_{O^*} - E_* - (E_{H2O} - E_{H2}) \quad (2)$$

$$H_2O + * \rightarrow HO^* + 1/2H_2, \quad \Delta E_{ads,HO^*} = E_{HO^*} - E_* - (E_{H2O} - 1/2E_{H2}) \quad (3)$$

$$2H_2O + * \rightarrow HOO^* + 3/2H_2, \quad \Delta E_{ads,HOO^*} = E_{HOO^*} - E_* - (2E_{H2O} - 3/2E_{H2}) \quad (4)$$

where E_*, E_{O^*}, E_{HO^*}, E_{HOO^*} are the ground state energies of the clean surface and that of the surfaces adsorbed with O*, HO*, and HOO*. E_{H2} and E_{H2O} are the calculated DFT energies of H_2 and H_2O molecules in the gas phase. In Fig. 2a the variation of HOO*/O*/HO* adsorption energies is plotted as a function of HO* adsorption energy. Linear

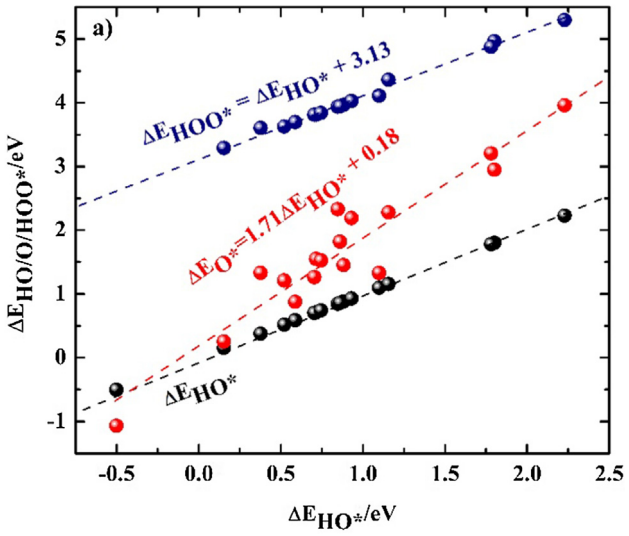

Fig. 2. Adsorption energies of HOO*/O*/HO* versus adsorption energies of HO*

correlations are obtained, with ΔE_{HOO^*} that is linearly related to that of ΔE_{HO^*} by $\Delta E_{HOO^*} = \Delta E_{HO^*} + 3.13$ eV, with the constant of approximate 3.13 eV that is independent of the binding strength to the surface. The slope unity in the linear fit is motivated by the single bond between O* and the carbon of the N-doped graphene sheet for both HO* and HOO* systems as further emphasized. All these data obey the universality scaling that was already shown for many materials with applications in both oxygen evolution reaction (OER) [32] and oxygen reduction reaction (ORR) [33]. A scaling relation is established also between ΔE_{HO^*} and ΔE_{O^*}, but with a slope that is close to two and with points that are more scattered than for ΔE_{HOO^*}. Definitely the slope indicates that oxygen binds differently than HO* and HOO* fragments and that indicates a larger change of ΔE_{O^*} when going from one structure to the other.

Therefore, we analyze systematically the variation of adsorption energies when going from one structure to the other as follows: when the nitrogen concentration (see in Fig. 1a the illustration of 1N, 2N, 3N) around the C active site increases, when one of the N nearest neighboring the C atom in the 2N structure is separated by 1/2/3C atom distance from it in different directions (see in Fig. 1b the structures − $2N_{1N-1Cd1}$, $2N_{1N-2Cd1}$, $2N_{1N-1Cd2}$, $2N_{1N-2Cd2}$, $2N_{1N-2Cd3}$, $2N_{1N-3Cd1}$) and when two nitrogen atoms out of the three nitrogen atoms nearest neighboring the C atom are moved at 1C atom distance away in two different directions (Fig. 1c the structures − $3N_{2N-1Cd1}$, $3N_{2N-1Cd2}$).

The energy difference between different adsorption energies as a function of environment around the active site is defined in a simplified manner as:

$$\Delta E_{diff} = \Delta E_{(HOO^*/O^*/HO^*),str1} - \Delta E_{(HOO^*/O^*/HO^*),str2} \quad (5)$$

where $\Delta E_{(HOO^*/O^*/HO^*),str1}$ and $\Delta E_{(HOO^*/O^*/HO^*),str2}$ are the adsorption energies of HOO*, HO*, O* fragments on different studied structures (i.e. $\Delta E_{diff,(x+1)N-xN}$ when the concentration increase around the active site x = (0–3)). For a better understanding, accross the paragraphs to the diff subscript, as a function of situation supplementary notation will be added.

As reference systems we considered the undoped graphene and the adsorption energy values calculated for the ideal catalyst (see the definition of ideal catalyst in the SI – shortly an ideal catalyst should be able to facilitate ORR above the equilibrium potential and all four charge transfer steps to have reaction free energy of the same magnitude at zero potential – 4.92 eV/4 = 1.23 eV and is equivalent to all reaction free energies being zero at the equilibrium potential and from there adsorption energies of HOO*/HO*/O* are calculated). Because on undoped graphene sheet during optimization the HOO* fragment flies away from the surface, we have used for comparison the value obtained for single point calculation when the fragment is in contact to the surface (see the black dashed line in Fig. 3a for HOO* on undoped sheet). The other two moieties, O* and HO* adsorb to the surface, with O* adsorbing on the bridge site between two C atoms and HO* ontop C site (structures not shown in Fig. 3a). When the G sheet is doped with 1N, the fragments bind to the carbon site next to the nitrogen. On these sites, their adsorption energies drop significantly compared to the undoped sheet – with energy differences of $\Delta E_{diff,0N-1N} = 1.36$ eV for HOO*, $\Delta E_{diff,0N-1N} = 1.63$ eV for O* and $\Delta E_{diff,0N-1N} = 1.38$ eV for HO* (see the differences between the energy levels of black and brown lines in Fig. 3a). All three fragments are stabilized with approximately the similar magnitude. When the second N is placed closed to the active site (2N structure), both HOO* and HO*continue to be stabilized (see dark blue line) with the same magnitude, but compared to the energy variations from 0N to 1N the magnitude is much lower ($\Delta E_{diff,1N-2N} \approx 0.65$ eV for 1N to 2N transition vs. $\Delta E_{diff,0N-1N} \approx 1.36$ for 0N to 1N transition). On the other hand the stabilization energy of O* is approximately 1.5 larger when the transition takes place from 1N to 2N configuration compared to transition from 0N to 1N. Moreover the magnitude is three time larger than that of HO*/HOO* ($\Delta E_{diff,O^*,1N-2N} = 2.07$ eV vs. ($\Delta E_{diff,HO^*/HOO^*,1N-2N} \approx 0.66$ eV).

When the active site is completely surrounded by nitrogen, the HOO* adsorbs under dissociated form: O* on the three coordinated nitrogen site and HO* next to the closest C atom adjoining one of the nitrogen atoms (during HOO* optimization HO detaches from O-see dark yellow line). For this fragment a direct comparison with adsorption on 1N and 2N structures cannot be done anymore. The adsorption energies of O* and HO* continues to strengthen, for O* with approx. 1.3 eV and for HO* with approx. 0.65 eV. Once more the rate with which O* adsorption energy increases is two times that of HO* when passing from 2N to 3N structure (1.32 eV for O* vs 0.65 eV for HO*). Compared to the transition from 1N to 2N the stabilization extent of O* is lower.

By comparing the adsorption energies with those of ideal catalyst, the adsorption energies on 1N surface are the closest, with ΔE_{HO^*} and ΔE_{O^*} that are similar with those of an ideal catalyst, while HOO* binds much more weakly than in the ideal case and is the one that gives the overpotential.

Summing up, the adsorption energies of O* increases much faster than that of the HO* and HOO* fragments, when the number of N atoms surrounding the active site increases (i.e. with approx. 5 eV for O* and 2.7 eV for HO* when going from 0N to 3N). If for 0N and 1N structures the O* is less stable than HO*, for 2N and 3N structures O* start to become more stable than the HO* fragment. This can be explained through the octet rule, as HO* and HOO* can accommodate 1 e^- while O* can accommodate 2e^- to form eight electron outer shells. The HOO*/HO* capturing abilities will become weak once the eight electron outer shells is formed. This could explain the different stabilization energies for O* and HO* and the fact that HOO* on 3N structures is not stable anymore with HO* that detaches and leaves only O* adsorbed on the active site. After HO* and HOO* complete their outer shells, if there is still available charge they won't accommodate anymore it, while O* will continue to capture the charge up to 2e^- (and the adsorption get strengthen as the charge is captured) such as to complete its outer shell. Similar trends were shown for the reducible metal oxide surfaces [34].

In the 2N structures in which one nitrogen atom is separated by 1C/2C/3C atoms sites from the active center, large variations of adsorption energies are registered as well (Fig. 3b). For the case of 1C site separation on two different directions ($2N_{1N-1Cd1}$ (blue dashed line), $2N_{1N-1Cd2}$ (blue short dashed line) in Fig. 2b), we observe that ΔE_{HO^*} and ΔE_{HOO^*} get very close to the adsorption energies registered for 1N surface, while ΔE_{O^*} is at approximately half the distance between binding on 1N structure and 2N, but slightly closer to 1N (see $\Delta E_{diff,O^*,0N-1N} \approx 0.88$–$0.78$ eV, $\Delta E_{diff,O^*,2N-3N} \approx 1.19$–$2.19$ eV in Fig. 3b). For the case when the N is separated by 2C sites apart from the active center – three different directions – $2N_{1N-2Cd1}$, $2N_{1N-2Cd2}$, $2N_{1N-2Cd3}$ (blue dashed, dash-dot and dotted lines in Fig. 3b) are possible. We observe that the same trend of variation for the adsorption energies of the fragments is obtained as in the case when the N is 1C site apart. Small variations of $\Delta E_{HOO^*}/\Delta E_{HO^*}$ depending on the directions in which the N was moved are found, while O* binds slightly weaker than when N is 1C apart (see in Fig. 3b connecting arrows that show ΔE_{diff} for $2N_{1N-2Cd2}$). For the case when N is at 3C atoms distance from the active site ($2N_{1N-3Cd1}$, Fig. 3b cyan dashed line)), ΔE_{O^*} approaches the adsorption energy value registered on 1N structure (compared with the case when this second N is at 1C/2C atoms distance from the active site). Even so, the $2N_{1N-3Cd1}$ is still approximately 0.5 eV more stable than the 1N case. No further tests have been performed for the case when N is 4C atoms sites apart from the active site. We suppose that, by extrapolating the trend, as the N-C distance increases the active sites will not feel anymore the effect of this N atom.

From these trends, it is concluded that O* is the fragment that feels the most the effect of the second N atom being placed at 1C/2C/3C sites apart from the active sites, and we assume this to be connected with the

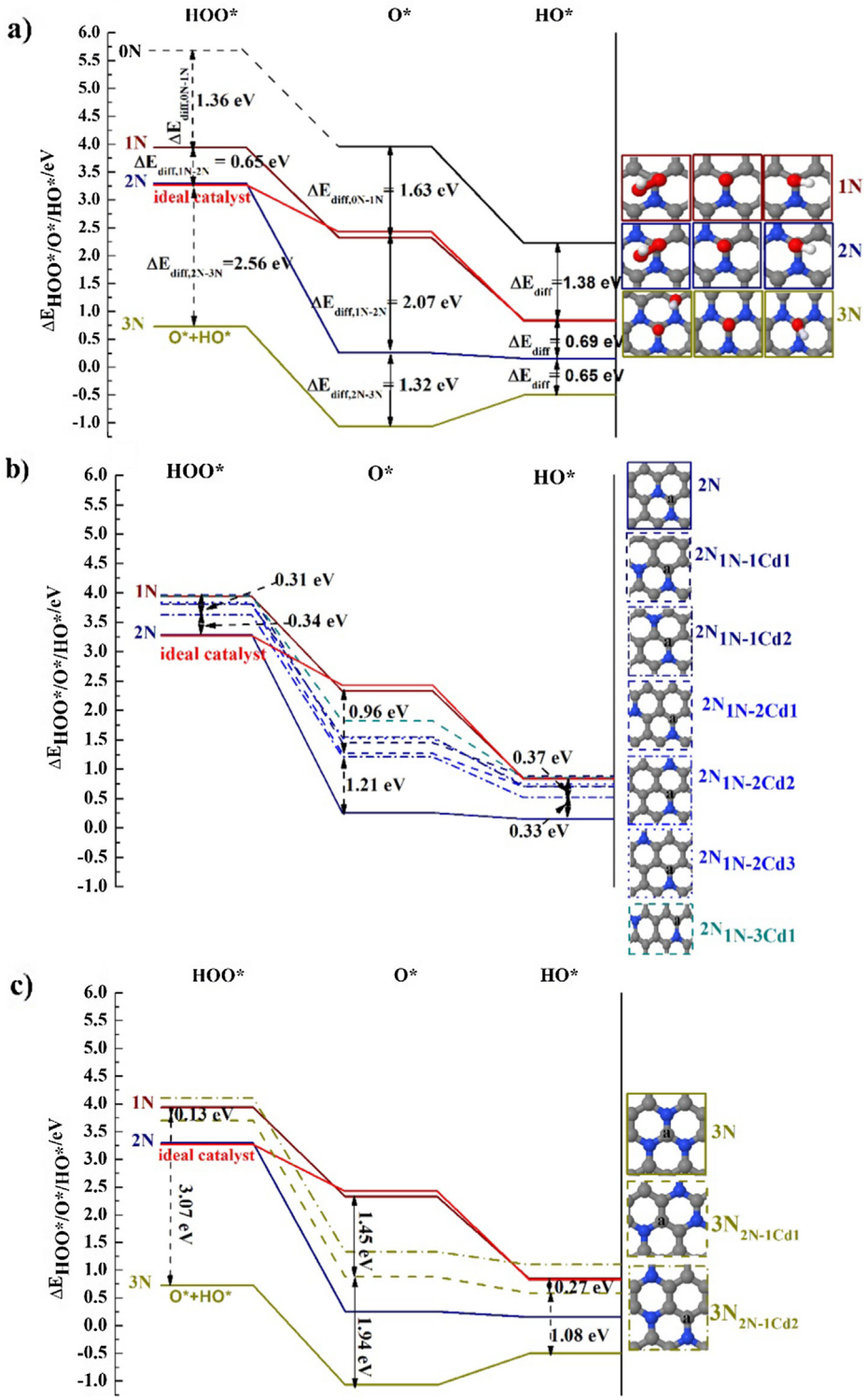

Fig. 3. Scheme for HOO*, O*, HO* adsorption energies variations (a) when passing from 1N, 2N and 3N doped G. In the right side of the graph – top view of O*, HO*, HOO* adsorbed structures. Color scheme of graphs: undoped G (black solid line), 1N doped (brown solid line), 2N (blue solid line), 3N (light green solid line), ideal catalyst (red solid line). The connecting arrows evidentiate three energy difference ($E_{diff,0N-1N/1N-2N/2N-3N}$) between adsorption energies on 0N − 1N − 2N − 3N structures; (b) in the 2N conformations when 1N atom is moved away from the active site by: 1C atom site apart in two directions − $2N_{1N-1Cd1}$ (dark blue dashed line), $2N_{1N-1Cd2}$ (dark blue short dashed line),by 2C atoms sites apart in three directions − $2N_{1N-2Cd1}$ (blue dashed line), $2N_{1N-2Cd2}$ (blue dashed dot line),$2N_{1N-2Cd3}$ (blue dotted line) and 3C atoms sites apart in one direction − $2N_{1N-3Cd1}$ (dashed dark cyan line) from the active site. The arrows indicate $\Delta E_{diff,1N-2N}$ between adsorption energies on 1N − $2N_{1N-2Cd2}$ − 2N surfaces and (c) in the 3N structure when two nearest neighbor nitrogen atoms are separated by 1C atom site each from the active center in two different directions $3N_{2N-1Cd1}$ (dashed light green line), $3N_{2N-1Cd2}$ (light green dashed dot line).The arrow indicate ΔE_{diff} between the adsorption energies on 1N − $3N_{2N-1Cd1}$-3N surfaces. Color code of top view of surfaces- C-gray, N-blue, O-red, H-white. The bold letter "a" –designates the active site). (For interpretation of the references to color in this figure legend, the reader is referred to the web version of this article.)

octet filling rule.

The last investigated configurations are those derived from 3N structure, when two nearest neighbor nitrogen atoms are separated by 1C site apart from the active center along two directions ($3N_{2N-1Cd1}$ and $3N_{2N-1Cd2}$ – see Fig. 3a). The general trend for $\Delta E_{HOO*}/\Delta E_{HO*}$ is the same as found for 2N type structures when one nitrogen is displaced from the active site. The adsorption energies get close to those obtained on the 1N structure (see the connecting arrows for $3N_{2N-2Cd1}$ structure). On $3N_{2N-2Cd1}$, HO* and HOO* adsorb slightly stronger than on the 1N, while on $3N_{2N-2Cd2}$ adsorb slightly weaker. ΔE_{O*} changes significantly, being placed close to the middle between 1N and 2N adsorption levels, varying with the displacement direction. It adsorbs stronger on $3N_{2N-1Cd1}$ than on $3N_{2N-1Cd2}$.

From these trends, it is concluded that O* is the fragment that feels the most the effect of the N atom placed at 1C/2C/3C sites apart from the active sites.

In Fig. 4a, 4b and 4c are plotted the density of states projected onto oxygen p states through which the three fragments bind to the surface. The increase of nitrogen content around the active site determine the shift of the states inside the valence band (see the p states for 1N (solid

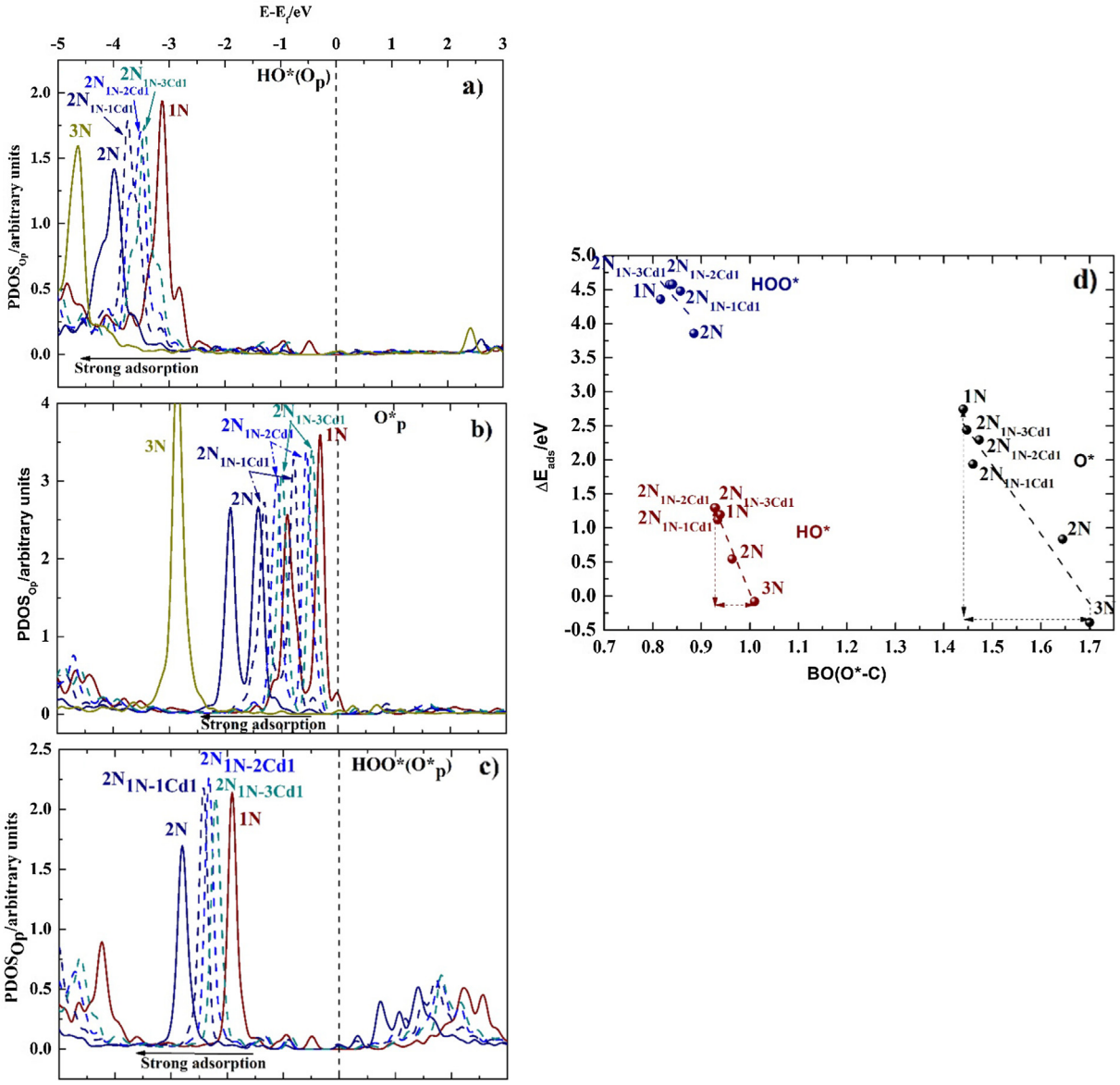

Fig. 4. PDOS onto oxygen p states of adsorbed intermediates on 3N, 2N, $2N_{1N-1Cd1}$, $2N_{1N-2Cd2}$, $2N_{1N-3Cd1}$, 1N. (a) HO*, (b) O*, (c) HOO* and (d) ΔE_{O^*} vs. C−*O bond order (black points), ΔE_{HO^*} vs. C−*OH bond order (brown points) and ΔE_{HOO^*} vs. C−*OOH bond order (blue points). (For interpretation of the references to color in this figure legend, the reader is referred to the web version of this article.)

brown line), 2N (dark blue solid line) and 3N (dark yellow solid line)). The shift is present also for the 2N type systems, when one of the 2N atoms is moved at different distances from the active site. When this distance increase (from 1C to 3C atoms distance), the oxygen p states shift from the 2N states – like case (when both N atoms are near the active center) towards the positioning of the p states as in the 1N structure.

The relation between the adsorption energies and the C−*O/*OH/*OOH bond orders are depicted in Fig. 4d. For both HO* and HOO* the bond order is close to 1, meaning that the fragment tend to form a single bond with the surface. HO* has the bond order slightly higher than that of HOO* fragments ((0.93–1.01) vs. (0.82–0.89)). A trend can be observed better for HO* than for HOO* because of the instability of HOO* fragment on the 3N structure. The adsorption energy increases with the increase of the bond order. The bond order for O* is higher than 1 and varies inbetween 1.44 and 1.77. For 2N and 3N structures the value is higher than 1.5 (1.64, 1.70), indicating that the O-C bond approaches a double bond character, while for 1N and the three structures with 1N separated by 1C/2C/3C sites from the active center ($2N_{1N-1Cd1}$, $2N_{1N-2Cd1}$, $2N_{1N-3Cd1}$), the values are slightly below 1.5 indicating a state of partially double bond state (1.44, 1.46, 1.47). The same correlation between the BO_{C-O^*} and ΔE_{O^*} with the increase of the adsorption energy with the bond order. Compared to HO* both the bond orders and adsorption energies increase with higher magnitudes (see the shape of triangles for HO* and O* formed between 1N and 3N structures). Similar variations of these fragments with the charge adsorbed from the TiO_2 semiconducting surface were found [34].

3.3. Co-adsorbate effect on the adsorption energies

It is expected that no matter on the solution pH, under steady state condition the N graphene surface to be covered with a certain amount of intermediates of reactions, such as O* or HO* or O*/HO*, which are in equilibrium with liquid water. On the other hand, the type of the intermediate is expected to depend among others on the pH.

On 1N surface, three active sites ($C_1/C_2/C_3$ – Fig. 5a) are possible. With increasing the nitrogen concentration increases the number of

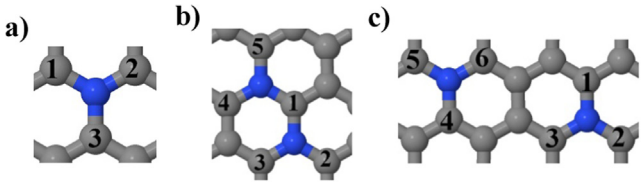

Fig. 5. The possible C active sites around N for the case of (a) 1N, (b) 2N and (c) $2N_{1N-3Cd1}$ models.

possible active sites that can be covered with intermediates. The question rises, if there is any influence of the co-adsorbate (i.e. found on C_2 on 1N structure) on the adsorption of reaction intermediate fragments (i.e. found on C_1 or C_3 for the 1N structure). In the following we analyze this influence on some representative structures (1N, 2N, $2N_{1N-3Cd1}$).

The results were obtained on surface models with coadsorbates placed on the same side of the sheet. Most of the tested models (HO*−HO*, HO*−O*, O*−O*, HOO*−O*, HOO*−HO*) on 1N, $2N_{1N-3Cd1}$ surfaces indicate that the structures with the fragments adsorbed on opposite facets are slightly less stable than when placed on the same side (see in Tables S2 and S3). This stability is given by the formation of hydrogen bonds between the fragments, even when the fragments are placed at larger distance. Therefore, in the first ORR step, the stabilization of the HOO* fragments will come, beside from the strength of the interaction with the active site also from the formation of hydrogen bonds with the co-adsorbates. The 1N and 2N surfaces free of co-adsorbates are taken as reference for comparison.

On the1N surface, because HO* is the fragment that binds the strongest on the active site (see the brown solid line in Fig. 2a), we will consider it the intermediate that presents a higher probability to be found as co-adsorbate under steady state conditions (i.e. adsorbed on C_2 site – notation $1N_{1HO}$). In this condition the adsorption energies of HOO*, O*, HO* intermediates are analyzed in Fig. 6. We observe that ΔE_{HOO*}, ΔE_{O*}, ΔE_{HO*} decrease considerably when compared to the case when the surface is free of coadsorbates ($\Delta E_{diff,coads\text{-}no\_coads} \approx 1$ eV for HOO* and HO* and 0.4 eV for O*). This is expected as they share the same pool of charge given by the single N atom. The C−OH bond order

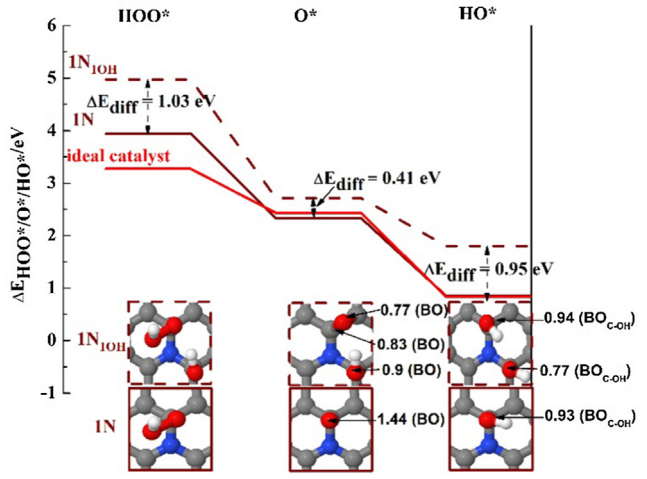

Fig. 6. Variation of adsorption energies for HOO*, O*, HO* on the 1N surface without (brown solid line) and with 1HO* coadsorbate ($1N_{1HO}$ – brown dashed line). Red solid line – the corresponding adsorption energies for the ideal catalyst. ΔE_{diff} values represent the difference between adsorption energies on 1N and $1N_{1HO*}$ surfaces. Top view of the surface structures color scheme – C-gray, N-blue, O-red, H-white. The numbers represent the bond orders C—O bond associated with the adsorbed fragments HO* and O*. (For interpretation of the references to color in this figure legend, the reader is referred to the web version of this article.)

values for the structure with two HO* fragments indicate that one of the frament has BO_{C-OH} similar with the case when is alone on the surface (0.94), while For the other HO* the BO_{C-OH} decreases considerably to 0.77. For the HO*−O* surface structure, the oxygen does not bind anymore ontop C but on the bridge position (see the surface top view in Fig. 6). For the structure with the O* ontop C, the BO_{C-O} decrease considerably to 1.11 (from 1.44). This leads to the O* migration on the bridge site and ends in a stabler structure with ≈0.25 eV. The HO* fragment keeps the same BO value as on the clean surface (0.95) when O* is ontop C. When O* is on the bridge position, two BOs values are present (corresponding to the binding to the two C atoms (0.77 and 0.83). From the total energy we observe also that O binds weaker than when it binds on the surface free of co-adsorbate. This could be explained by the bridge position that is different than ontop. On the same surface the BO_{C-OH} of HO* fragment decreases slightly to 0.9.different way of adsorption.

For the 2N representatives (2N and $2N_{1N-3Cd1}$) the existence of co-adsorbates on other active sites is inevitable. The same is valid for the models with higher N concentration.

On the 2N structure there are two types of active sites and the total number of C atoms that could be active is 5 (see Fig. 5b). C_1 is the most active site because has two next-neighbor N atoms. The other four are equivalent since each is adjoining one N. Therefore we have investigated two possible cases. One is when C_1 is the site where the reaction takes place while on one of the other active sites ($C_{2/3/4/5}$), 1O* ($2N_{2N*-1N(O)}$ structure, 2N*−1N(1O) subscript means the reaction takes place on the C neighbor to 2N and 1O is co-adsorbed on the site that is adjoining 1N) or 1HO*($2N_{2N*-1N(1HO)}$ structure, 2N*- 1N (1OH) subscript means that the reaction take place on C adjoining 2N atoms and HO* is adsorbed on the site that is adjoining 1N) intermediates are co-adsorbed (see top view of surfaces in Fig. 7a). The other one is when C_2 (or $C_{3/4/5}$) is the site where the reaction takes place and C_1 is occupied with the 1O* ($2N_{1N*-2N(1O)}$) or with 1HO*($2N_{1N*-2N(1OH)}$) intermediates (1N*−2N(1O)/1N*−2N(1OH) subscript means that the reaction takes place on the site adjoining 1N and the co-adsorbate occupy the site adjoining 2N- see the top view of the investigated surfaces in Fig. 5b). We have considered both O* and HO* as potential coadsorbates, as both adsorb strong. Depending on reaction conditions (eg. pH) each of them could be present on the surface.

When the reaction site is C_1 and on C_2 are the co-adsorbates, the adsorption energies of all intermediates on this site decrease in the order: $\Delta E_a(2N) > \Delta E_a(2N_{2N*-1N(1OH)}) > \Delta E_a(2N_{2N*-1N(1O)})$ (Fig. 7a). If for 1HO* coadsorbate, the adsorption energies of intermediates are approximately in-between 2N and 1N levels, for 1O* co-adsorbate the O* level on the reaction site is already the same as on 1N, while HO* and HOO* adsorb weaker than on 1N. Therefore, O* destabilize in a much higher extent the intermediates than HO*.

Because C_2 sites adjoin only 1N (see Fig. 7b) the intermediates bind weaker than on C_1 even when the other C active sites are free from intermediates (HO* and HOO* bind with approximately 0.5 eV weaker on C_2 than on C_1, while O* with approximately 0.9 eV weaker). The adsorption trend when 1HO* and 1O* are preadsorbed is the same as for the previous case: ΔE_a ($2N_{1N*}$) > ΔE_a ($2N_{1N*-1OH(2N)}$) > ΔE_a ($2N_{1N*-1O(2N)}$). For 1HO co-adsorbate the energy levels shift to the same level as for 1N system, while for 1O* the energy levels already shifts towards much weaker adsorption energies for all intermediates.

This trend of significant weakening of the adsorption energies of the intermediates when going from free of adsorbates surfaces to pre-adsorbed HO* and further to O* co-adsorbates, can be explained as well by the HO* and O* capacities to accommodate charges in the context of charge sharing. Thus, HO* which require less charge than O*, leaves more charge for the active site and affects less the adsorption energies on the reaction sites.

For the $2N_{1N-3Cd1}$ structure (see Fig. 7c) all six possible active sites are equivalent because the two N are at aproximately 5 Å side appart

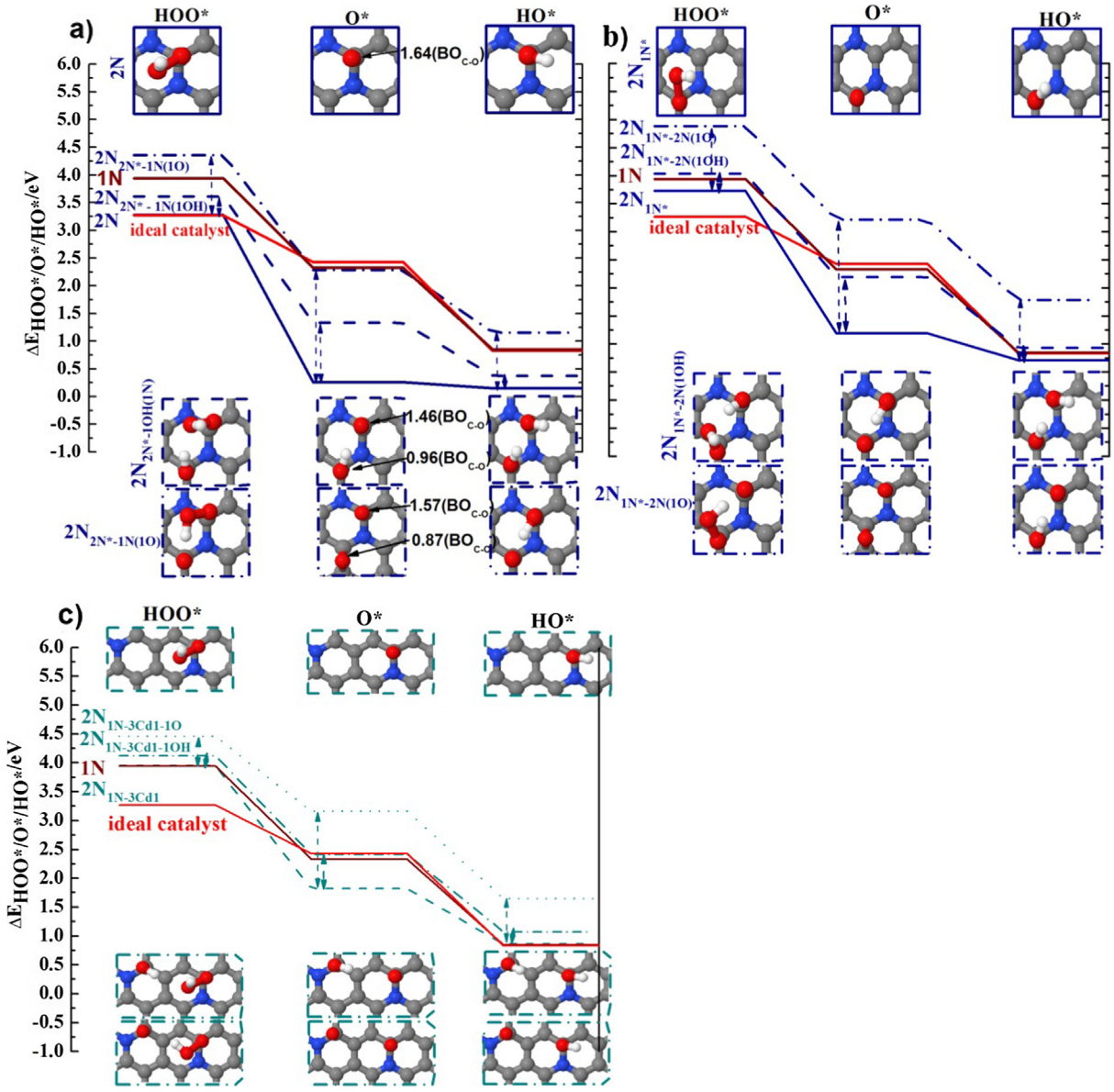

Fig. 7. Variation of adsorption energies for HOO*, O*, HO* with 1O* or 1HO* as co-adsorbates on (a) 2N, when the active site is the C adjoining two N atoms (C_1) and the co-adsorbate is adjoining one N atom (C_2), (b) $2N_{1N*}$, when the active site is the C adjoining one nitrogen atom (C_2) and the co-adsorbate is adjoining the 2N (C_1) and (c) $2N_{1N-3Cd1}$, when the active site and the co-adsorbate each are adjoining 1N.

and each has its own three active sites. The co-adsorbate fragments were placed on C_6 (next to one nitrogen atom), while the reaction takes place on C_1 (next to the other nitrogen atom). In this adsorption configuration the charge sharing is maximized (is the most stable configuration), because each fragment benefits from adjoining one N, each and are close enough to form hydrogen bonds. At this distance, as shown in the previous chapter, the activity of the sites gets closer to that on 1N system in terms of HO* and HOO* adsorption energies and with O* that binds stronger (cyan solid line in Fig. 7c). The variation of adsorption energies of intermediates follow the same trend, as emphasezied in the previous paragraph, when going from clean to HO* and O* co-adsorbates: 2N > $2N_{1N-3Cd1-1OH}$ > $2N_{1N-3Cd1-1O}$ (see the differences between solid – dashed and dot dashed lines in Fig. 7c). The HO* and HOO* adsorption energies are slightly weakened by the 1HO* co-adsorbate, while O* level is brought to the same value as obtained on 1N free of co-adsorbate (cyan dashed line). On the other hand O* continue to destabilze the intermediates (cyan dashed dot line) with a higher magnitude than HO*.

The overall conclusion is that the presence of co-adsorbates on the other active sites influence quite significantly the adsorption energies, almost with the same magnitude with which the concentration of N atoms around the active sites does, but the shift is towards weaker values acting as a counterbalance to the N effect. Compared to the ideal catalyst, the investigated structures $2N_{1N-3Cd1-1OH}$ and $2N_{N*-2N(1OH)}$ have the HO*/O* adsorption energy levels close to those of the ideal catalyst, but as in the case of the 1N structure, HOO* binds much more weaker than in the ideal case. To get closer to ideal levels, HO* and O* should be kept at the same level and the adsorption energy of HOO* should be strengthened.

3.4. Theoretical overpotential

In this section, based on the thermodynamic model proposed by Nørskov et al. [35], we have calculated the free energies of the reaction intermediate steps. We determined the least exothermic step (the rate limiting step) that gives the overpotential for ORR (Eqs. (6)–(9) and

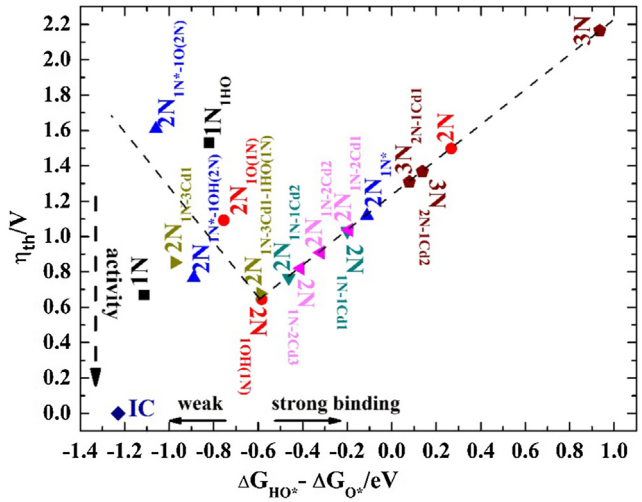

Fig. 8. Volcano plot – general activity trends for ORR theoretical overpotential (η_{th}) vs. standard free energy of the oxygen protonation step ($\Delta G_{HO^*} - \Delta G_{O^*}$). IC represents the point for the ideal catalyst.

explained in SI). The theoretical overpotential is derived only from the adsorption energies of intermediates without including other stabilization effects such as water.

We consider the oxygen reduction cycle through the four-electron process with the following elementary steps:

$$O_2 + (H^+ + e^-) + * \rightarrow HOO^* \quad \Delta G1 = \Delta G_{HOO^*} - \Delta G_{O2} \tag{6}$$

$$HOO^* + (H^+ + e^-) \rightarrow O^* + H2O(l) \quad \Delta G_2 = \Delta G_{O^*} - \Delta G_{HOO^*} \tag{7}$$

$$O^* + (H^+ + e^-) \rightarrow HO^* \quad \Delta G_3 = \Delta G_{HO^*} - \Delta G_{O^*} \tag{8}$$

$$HO^* + (H^+ + e^-) \rightarrow * + H_2O(l) \quad \Delta G_4 = -\Delta G_{HO^*} \tag{9}$$

where $\Delta G_{1/2/3/4}$ are the free energies of the respective intermediate steps and $\Delta G_{HOO^*/O2/O^*/HO^*}$ are the free energies of intermediates. The way they are calculated is detailed in SI.

A volcano plot was built (Fig. 8) using as a descriptor the free energy of the deprotonation step: $\Delta G_{HO^*} - \Delta G_{O^*}$. Compared to the other descriptor used in literature so far (ΔG_{HO^*}) [33,36], this one describes better the activity for most of our systems, because of the large variations between ΔE_{O^*}- ΔE_{HO^*} when passing from one system to the other. The most active sites are the ones that are close to the top of the volcano (as much as possible close to the 0 value of theoretical overpotential and which is represented by the ideal catalyst – IC). The point for the ideal catalyst was placed as well in the plot (the IC point). Even the best performing point is still far from the ideal. On the right side of the volcano the trends are smooth because this descriptor is the rate limiting step. On the left side of the volcano some points are not well described by this descriptor – mostly because of different limiting step.

Analyzing the trends the overpotential decreases as the N concentration around the active site decreases $\eta_{th,3N} > \eta_{th,2N} > \eta_{th,1N}$. For 1N system the overpotential is around 0.67 eV, among the best ones when compared with the other systems. It decreases as well when one of the two N atoms adjoining the C active site, starts to be separated by the active center by 1/2/3C atoms sites. The overpotentials for $2N_{1N-1/2Cd1/2/3}$ systems are placed on the strong binding site of the volcano, while for $2N_{1N-3Cd1}$ the overpotential is already placed on the weak binding side of the volcano and gets closer to the 1N overpotential point. This shows that if the second N is placed at a distance larger than 5 Å from the other N, its effect will not be felt anymore by the active site and the system will behave as 1N system. For the $3N_{2N-1Cd1/2}$ systems, that have the active site next to 1N and the other two N moved 1C site apart from it, the overpotential decrease significantly compared to 3N system (from 2.17 eV to 1.31/1.36 eV).

For the studied systems, the presence of one of the co-adsorbate intermediates (HO*/O*) on one of the other active sites influences quite significantly the overpotential. On $1N_{1HO}$ system the overpotential increases, because they share the same N and the adsorption energies of all intermediate decreases. The potential determining step stays as well the formation of HOO* moiety.

For the 2N and $2N_{1N^*}$ models, the overpotentials decrease significantly and move towards the top of the volcano for 1HO* co-adsorbate, while for O* the overpotentials increase again. On $2N_{1N-3Cd1}$, the HO* co-adsorbate decreases as well the overpotential when compared to the free co-adsorbate systems, while O* increases it. If more co-adsorbates are supposed to adjoin the same N, by extrapolation using the 1N model, the overpotential is predicted to increase. Similar variations are supposed to take place on the 3N systems when co-adsorbates are present. Therefore, the overpotential of the active site surrounded by 2/3N atoms is increased due to the high amount of charge provided by nitrogen, but the ORR intermediates that are highly possible to co-adsorb on the other active sites, depending on the co-adsorbate type and the adsorption site, could decrease the overpotential more or less.

3.5. Water effect

As mentioned in literature, the interaction between water molecules and intermediates affects the stability of surface species on N-graphene. This effect can vary for example with the number of hydrogen bonds between water molecules and the intermediates, with the electrolyte pH near the electrode, with the presence of other ions in solution etc. Because the purpose of this study is focused on the variation of adsorption energies of ORR intermediates in the absence of water, we use the stabilization energies given in the literature to check the overpotential trends. Yu et al. [10] found a stabilization energy of −0.42 eV for HO*, −0.53 eV for O* and −0.49 eV for HOO*. Thus, all of them are stabilized almost with the same magnitude. Reda et al. [13] obtained slightly smaller stabilization energies: −0.20 eV for HO*, −0.38 eV for O* and −0.19 eV for HOO*. Because these reported stabilization energies are slightly different, both of them were applied to our data and the obtained volcano plots are depicted in Fig. 9. Other stabilization values can be present as well, due to the solution pH, an aspect that is less studied theoretically.

The stabilizing effect makes the points to shift towards stronger binding but the general trends concerning the overpotential when passing from one system to another are kept. The overpotentials are slightly lower when using M. Reda values, which is due to the fact that there is a higher stabilizing difference between O* and HO* which will increase the exothermicity of the rate limiting step. The stabilization effects increase will rise the probability of existence of more co-adsorbates around the N active sites. An example is the 1N system free of co-adsorbates. When applying the stabilizing effect of water, with both sets of values, a much smaller overpotential is obtained compared to the reported experimental value (0.3/0.41 eV vs. 0.4 eV [37]). When the 1HO* is co-adsorbed, the overpotential increases to 0.72/0.92 eV.

4. Conclusions

By using DFT calculations we analyzed the variation of adsorption energies of ORR intermediates with increasing N concentration around the C active sites on the basal plane of graphene sheet (1N that means 33% around the active site, 2N-67%, 3N-100%). It was found that with the increasing of N concentration, O* adsorption energy decrease faster than that of HO*/HOO* (5 eV vs 2.7 eV when going from 0N to 3N atoms adjoining the active site). This variation was explained with the aid of C–O* bond order investigation, which shows that the bond order for O* varies with increasing the concentration, from single to partially double and to double bond, while for HO* and HOO* gets closer to single bond and is according to the octet rule to fill the outer shell to

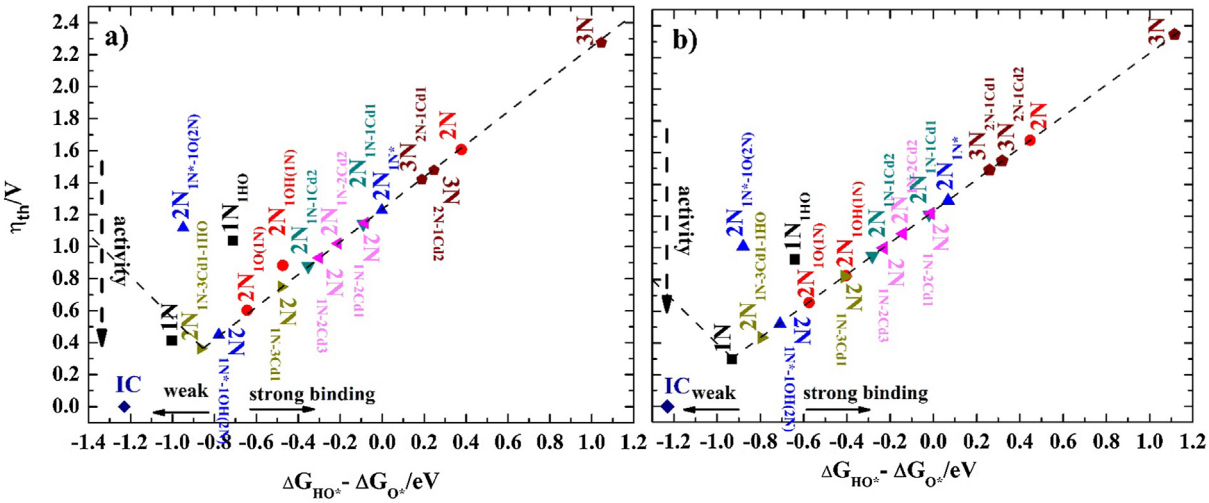

Fig. 9. Volcano plot – general activity trends for ORR theoretical overpotential (η_{th}) vs standard free energy of the oxygen protonation step ($\Delta G_{HO^*} - \Delta G_{O^*}$) with water stabilization energies applied to HOO*, O*, HO* intermediates from (a) Ref. [10] and (b) Ref. [13].

form eight electron outer shell. Therefore this different way of the fragments to accumulate the charge (with O* that accommodate more charge than HO*/HOO*) makes the O* adsorption energy to strengthen with a significant higher magnitude than HO* and this mirror in the variation of the theoretical overpotential when going from one structure to the other.

In the 2N structures by separating one of the adjoining N atoms by 1C/2C/3C sites from the active center, its effects on HO*/HOO*/O* decrease considerably. When is only 1C site apart, the adsorption energies of HOO*/HO* are similar to those on the system with 1N, while the O* can still feel the presence of N even from 3C sites apart. As a general conclusion, the trends of the adsorption energies variations are affected beside the amount of charge provided by increasing the N concentration, also by the amount of charge the HO*/HOO*/O* intermediates can accommodate.

The same trend of variations was obtained for O* and HO* co-adsorbates when placed on other possible active sites. On the 2N systems that were studied for co-adsorbate effect, O* weakens the adsorption energies of the intermediates on the reaction site with a much higher magnitude than HO* (up to 2 eV for O* co-adsorbate vs. 1 eV for HO* co-adsorbate relative to the free of co-adsorbate surfaces).

All these variations are mirrored in the theoretical overpotential that increase with the N concentration (1N > 2N > 3N). For the same concentration (2N) it decreases in the presence of 1HO* co-adsorbate and increase again in the presence of O*, but is not higher than when no co-adsorbate is present. The overpotential decreases and approaches to the overpotential on 1N when one of the 2N atoms is displaced by 1C/2C/3C atoms from the active site. Similar significant decrease of overpotential is found when two N out of three N are moved 1C site from the active site.

The effect of water was studied using corrections from two different studies. The activity trends remain the same, but due to stabilizing effects on the adsorbed species, the change of surface coverage with HO* and O* fragments is expected. This will affect the adsorption energies of ORR intermediates and at their turns affects the overpotential towards lower or higher values when compared to free of co-adsorbates surfaces (i.e. on $1N_{1HO^*}$ structure during the reaction one of the three active sites will have co-adsorbed 1HO* and the reaction will take place on one of the other two active sites- with an increase of overpotential compared to the case when no co-adsorbates are present).

The overall conclusion is that not only the N concentration and their distance from the active site are the one that influence the adsorption energy of ORR intermediates on the N doped graphene, but also the capacity of the intermediates to accumulate charge (i.e. O* more than HO*) that affects quite significantly and differently the magnitude of adsorption energy variations. The present results are expected to provide insights concerning the relation between N concentration and the amount of charge the adsorbate/co-adsorbate can accommodate on N doped graphene which is mirrored in the final values of adsorption energies and in the final activity for the ORR application, when the clustering phenomenon takes place locally during synthesis. These trends are expected to be extrapolated to other types of intermediates and dopants that accept or provide different amount of charge.

CRediT authorship contribution statement

Isabela-Costinela Man: Conceptualization, Data curation, Formal analysis, Project administration, Supervision, Writing - original draft, Writing - review & editing. **Ionut Trancă:** Conceptualization, Data curation, Formal analysis, Methodology, Software, Writing - review & editing. **Stefan-Gabriel Soriga:** Software, Methodology, Data curation.

Declaration of Competing Interest

The authors declare that they have no known competing financial interests or personal relationships that could have appeared to influence the work reported in this paper.

Acknowledgements

This work was supported by UEFISCDI project number PN-III-P1-1.1-TE-2016-2191, nr. 89/2018.

Appendix A. Supplementary material

Supplementary data to this article can be found online at https://doi.org/10.1016/j.apsusc.2020.145470.

References

[1] T. Granzier-Nakajima, K. Fujisawa, V. Anil, M. Terrones, Y.T. Yeh, Controlling nitrogen doping in graphene with atomic precision: Synthesis and characterization, Nanomaterials 9 (3) (2019).
[2] Z. Luo, et al., Pyridinic N doped graphene: synthesis, electronic structure, and electrocatalytic property, J. Mater. Chem. 21 (22) (2011) 8038–8044.
[3] K. Gong, et al., Nitrogen-doped carbon nanotube arrays with high electrocatalytic activity for oxygen reduction, Science 323 (5915) (2009) 760–764.
[4] L. Qu, et al., Nitrogen-doped graphene as efficient metal-free electrocatalyst for oxygen reduction in fuel cells, ACS Nano 4 (3) (2010) 1321–1326.
[5] S.K. Singh, K. Takeyasu, J. Nakamura, Active sites and mechanism of oxygen

reduction reaction electrocatalysis on nitrogen-doped carbon materials, Adv. Mater. 31 (13) (2019) 1804297.
[6] C.H. Choi, et al., Long-range electron transfer over graphene-based catalyst for high-performing oxygen reduction reactions: importance of size, N-doping, and metallic impurities, J. Am. Chem. Soc. 136 (25) (2014) 9070–9077.
[7] D. Guo, et al., Active sites of nitrogen-doped carbon materials for oxygen reduction reaction clarified using model catalysts, Science 351 (6271) (2016) 361–365.
[8] G.W. Crabtree, M.S. Dresselhaus, The hydrogen fuel alternative, MRS Bull. 33 (4) (2011) 421–428.
[9] Y. Okamoto, First-principles molecular dynamics simulation of O2 reduction on nitrogen-doped carbon, Appl. Surf. Sci. 256 (1) (2009) 335–341.
[10] L. Yu, et al., Oxygen reduction reaction mechanism on nitrogen-doped graphene: A density functional theory study, J. Catal. 282 (1) (2011) 183–190.
[11] W.A. Saidi, Oxygen reduction electrocatalysis using N-doped graphene quantum-dots, The Journal of Physical Chemistry Letters 4 (23) (2013) 4160–4165.
[12] G.-L. Chai, et al., Active sites and mechanisms for oxygen reduction reaction on nitrogen-doped carbon alloy catalysts: stone-wales defect and curvature effect, J. Am. Chem. Soc. 136 (39) (2014) 13629–13640.
[13] M. Reda, H.A. Hansen, T. Vegge, DFT study of stabilization effects on N-doped graphene for ORR catalysis, Catal. Today 312 (2018) 118–125.
[14] D. Kwak, et al., First principles study of morphology, doping level, and water solvation effects on the catalytic mechanism of nitrogen-doped graphene in the oxygen reduction reaction, ChemCatChem 6 (9) (2014) 2662–2670.
[15] A. Ferre-Vilaplana, E. Herrero, Charge transfer, bonding conditioning and solvation effect in the activation of the oxygen reduction reaction on unclustered graphitic-nitrogen-doped graphene, PCCP 17 (25) (2015) 16238–16242.
[16] P. Zhang, et al., Size effect of oxygen reduction reaction on nitrogen-doped graphene quantum dots, RSC Adv. 8 (1) (2018) 531–536.
[17] X. Zou, L. Wang, B.I. Yakobson, Mechanisms of the oxygen reduction reaction on B- and/or N-doped carbon nanomaterials with curvature and edge effects, Nanoscale 10 (3) (2018) 1129–1134.
[18] A. Hjorth Larsen, et al., The atomic simulation environment—a Python library for working with atoms, J. Phys.: Condens. Matter 29 (27) (2017) 273002.
[19] J. Enkovaara, et al., Electronic structure calculations with GPAW: a real-space implementation of the projector augmented-wave method, J. Phys.: Condens. Matter 22 (25) (2010) 253202.
[20] H.J. Monkhorst, J.D. Pack, Special points for Brillouin-zone integrations, Phys. Rev. B 13 (12) (1976) 5188–5192.
[21] J. Wellendorff, et al., Density functionals for surface science: Exchange-correlation model development with Bayesian error estimation, Phys. Rev. B 85 (23) (2012) 235149.
[22] G. Kresse, J. Furthmüller, Efficiency of ab-initio total energy calculations for metals and semiconductors using a plane-wave basis set, Comput. Mater. Sci. 6 (1) (1996) 15–50.
[23] G. Kresse, J. Hafner, Ab initio molecular-dynamics simulation of the liquid-metal–amorphous-semiconductor transition in germanium, Phys. Rev. B 49 (20) (1994) 14251–14269.
[24] G. Kresse, J. Furthmüller, Efficient iterative schemes for ab initio total-energy calculations using a plane-wave basis set, Phys. Rev. B 54 (16) (1996) 11169–11186.
[25] G. Kresse, D. Joubert, From ultrasoft pseudopotentials to the projector augmented-wave method, Phys. Rev. B 59 (3) (1999) 1758–1775.
[26] T.A. Manz, Introducing DDEC6 atomic population analysis: part 3. Comprehensive method to compute bond orders, RSC Adv. 7 (72) (2017) 45552–45581.
[27] T.A. Manz, N.G. Limas, Introducing DDEC6 atomic population analysis: part 1. Charge partitioning theory and methodology, RSC Adv. 6 (53) (2016) 47771–47801.
[28] N.G. Limas, T.A. Manz, Introducing DDEC6 atomic population analysis: part 2. Computed results for a wide range of periodic and nonperiodic materials, RSC Adv. 6 (51) (2016) 45727–45747.
[29] R.A. van Santen, I. Tranca, How molecular is the chemisorptive bond? PCCP 18 (31) (2016) 20868–20894.
[30] R.A. van Santen, I. Tranca, E.J.M. Hensen, Theory of surface chemistry and reactivity of reducible oxides, Catal. Today 244 (2015) 63–84.
[31] W. Yang, T.-P. Fellinger, M. Antonietti, Efficient metal-free oxygen reduction in alkaline medium on high-surface-area mesoporous nitrogen-doped carbons made from ionic liquids and nucleobases, J. Am. Chem. Soc. 133 (2) (2011) 206–209.
[32] I.C. Man, et al., Universality in oxygen evolution electrocatalysis on oxide surfaces, ChemCatChem 3 (7) (2011) 1159–1165.
[33] M. Li, et al., N-doped graphene as catalysts for oxygen reduction and oxygen evolution reactions: theoretical considerations, J. Catal. 314 (2014) 66–72.
[34] X. Huang, et al., An essential descriptor for the oxygen evolution reaction on reducible metal oxide surfaces, Chem. Sci. 10 (11) (2019) 3340–3345.
[35] J. Rossmeisl, A. Logadottir, J.K. Nørskov, Electrolysis of water on (oxidized) metal surfaces, Chem. Phys. 319 (1) (2005) 178–184.
[36] F. Calle-Vallejo, J.I. Martínez, J. Rossmeisl, Density functional studies of functionalized graphitic materials with late transition metals for oxygen reduction reactions, PCCP 13 (34) (2011) 15639–15643.
[37] C.H. Choi, S.H. Park, S.I. Woo, Binary and ternary doping of nitrogen, boron, and phosphorus into carbon for enhancing electrochemical oxygen reduction activity, ACS Nano 6 (8) (2012) 7084–7091.